Surface morphological evolution during annealing of epitaxial Cu(001) layers

J. M. Purswani and D. Gall[a)]
Department of Materials Science and Engineering, Rensselaer Polytechnic Institute, Troy, New York 12180, USA

(Received 2 April 2008; accepted 16 June 2008; published online 22 August 2008)

Single crystal Cu(001) layers were grown on MgO(001) by ultrahigh vacuum magnetron sputtering at $T_s = 100$ °C. Quantitative surface morphological analyses by *in situ* scanning tunneling microscopy show that the surfaces exhibit self-affine mound structures with a scaling exponent of 0.82 ± 0.03 and a mound radius r_c that increases from 31 ± 8 to 39 ± 6 nm for increasing layer thickness $t = 24$–120 nm. *In situ* annealing at 200 and 300 °C leads to a thermodynamically driven mass transport that minimizes the surface step density, resulting in broader mounds and a smaller root mean square surface roughness σ. This effect is most pronounced for $t = 24$ nm, for which r_c increases from 31 ± 8 to 70 ± 20 nm and σ decreases from 1.3 ± 0.1 to 0.74 ± 0.08 nm, resulting in a decrease in the average surface slope from $\chi = 7°$ to $2°$ and an increase in the average terrace width w_T by more than a factor of 4. In contrast, w_T increases by only 20% for $t = 120$ nm. This remarkable difference between "thin" and "thick" layers is attributed to diverging surface morphological pathways during annealing: The strong smoothening for $t = 24$ nm is due to a competitive coalescence process where some mounds grow laterally at the expense of their smaller neighbors, which die out. In contrast, the initially wider mounds of thicker layers ($t = 120$ nm) combine to form a quasistable surface morphology that exhibits anisotropic mound structures, which limit mass transport and stabilize the surface step density. © *2008 American Institute of Physics*.
[DOI: 10.1063/1.2968440]

I. INTRODUCTION

Single crystal copper layers are of interest as seed layers for magnetic devices,[1–3] catalysts,[2,4,5] and optical coatings,[6] as well as for the study of the mechanisms governing electromigration[7] and surface scattering.[8–10] A detailed understanding of the processes that determine the microstructural and surface morphological evolution is critical for these applications and the development of a process that controllably alters the surface morphology is desirable. Various researchers have grown epitaxial Cu on Si(001),[9,11–16] Si(111),[7,13,17] and MgO(001),[6,18,19] and have studied the microstructure by x-ray[3,8,9,13–16,19] and electron diffractions,[1,6,8,12–17,20,21] and the surface morphology by *ex situ* atomic force microscopy, which is, however, affected by surface oxidation.[22] Epitaxial Cu(001) layers grown on hydrogen-terminated Si(001) by thermal evaporation at room temperature exhibit atomically rough surfaces with 5–30 nm wide mounds and a root mean square (rms) roughness of 1–2 nm. Subsequent annealing at $T_a \geq 50$ °C causes additional surface roughening and $T_a \geq 200$ °C leads to silicide (Cu_3Si) formation.[9] These results were confirmed by other researchers using *in situ* scanning tunneling microscopy (STM) showing monoatomic height surface steps of Cu(001) on H-terminated Si(001), a rms roughness of 0.9 nm, and a lateral correlation length ξ of 16 nm.[1] Cu layers evaporated on MgO(001) exhibit larger ξ values,[1] which show a maximum at an intermediate growth temperature $T_s \sim 150$ °C and increase with a decreasing growth rate.[2] We have recently shown that T_s for the growth of epitaxial Cu(001)/MgO(001) is limited to <200 °C.[19] At higher temperatures, the Cu layers are polycrystalline since temperature-induced mass transport allows Cu nuclei to sample the orientational space and find lower energy (and/or lower lattice mismatch) configurations, leading to a mixture of 001, 203, and $\bar{1}75$-oriented grains.[19] However, the limited adatom mobility at $T_s = 100$ °C leads to kinetic roughening and surfaces that exhibit a high density of surface steps, which, in turn, are expected to be responsible for diffuse electron surface scattering.[10]

Here we report on the surface morphological evolution during *in situ* postdeposition annealing of single crystal Cu/MgO(001) layers, showing a dramatic reduction in the surface step density and a correlated increase in the average (atomically smooth) terrace width w_T. Height-height and autocorrelation analyses from STM micrographs of as-deposited ($T_s = 100$ °C) as well as annealed Cu(001) layers show an increase in the mound radius r_c and a decrease in the rms surface roughness σ upon annealing at 200 and 300 °C. This effect is most pronounced for thin layers ($t = 24$ nm), for which w_T increases by more than a factor of 4. In contrast, w_T increases by only 20% for $t = 120$ nm. This dramatic difference is attributed to a change in the surface mass transport, which leads to competitive mound coalescence for small t but anisotropic quasistable mounds for higher t. The annealed single crystal Cu surfaces may become useful for various applications mentioned above, which will benefit from atomic level smoothness.

[a)]Electronic mail: galld@rpi.edu.

 © 2008 American Institute of Physics

Author complimentary copy. Redistribution subject to AIP license or copyright, see http://jap.aip.org/jap/copyright.jsp

II. EXPERIMENTAL PROCEDURE

Copper layers were grown in a load-locked UHV dc magnetron sputtering system with a base pressure of 1.3×10^{-7} Pa (1×10^{-9} Torr), achieved by a $520\ \mathrm{l\,s^{-1}}$ turbomolecular pump. The substrates were single-side polished $10\times 10\times 0.5\ \mathrm{mm}^3$ MgO(001) wafers, cleaned with successive ultrasonic baths of trichloroethylene, acetone, and isopropanol, rinsed with de-ionized water, and then blow dried with dry nitrogen.[23] A conductive contact was painted from the front to the back of the substrates, using colloidal graphite, in order to ensure electric contact during STM analyses. The samples were then secured to a stainless steel backing plate by mechanical clamping and by silver paint, which was cured on a hot plate at 150 °C for 10 min. The backing plates were mounted to a molybdenum holder and inserted into the load-lock system for transfer to the growth chamber. The substrates were subjected to thermal degassing for 1 h at 800 °C, which has been shown to result in clean MgO(001) surfaces for epitaxial growth.[24,25] The temperature was measured by a *K*-type thermocouple located within the sample stage and confirmed by optical pyrometry.

Prior to deposition, the substrate and stage were allowed to cool to the deposition temperature T_s=100 °C. Ar (99.999% pure) was further purified through a Micro Torr purifier and introduced into the deposition chamber to provide a constant pressure of 0.33 Pa (2.5 mTorr), as measured with a capacitance manometer. Sputtering was done using a water-cooled 75-mm-diameter copper target (99.999% pure) facing the substrate at a distance of 12 cm. Immediately before deposition, the target was sputter cleaned for 5 min with a protective shield covering the substrate. Layers were grown at a constant power of 150 W, resulting in a growth rate of ~40 nm/min, as determined using cross-sectional scanning electron microscopy (SEM) on calibration samples.

After deposition, the samples were allowed to cool to <70 °C before they were transferred to the analysis chamber without breaking vacuum. The base pressure of the analysis system was less than 1.3×10^{-7} Pa (1×10^{-9} Torr) maintained with a $300\ \mathrm{l\,s^{-1}}$ ion pump. The sample surface morphology was characterized using *in situ* STM, utilizing a commercially prepared tungsten tip. Samples were scanned at a bias voltage of 0.33 mV and a constant tunneling current of 0.6 nA. After the initial STM analysis, the layers were transferred to the growth chamber where they were annealed for 30 min at T_a=200 or 300 °C. The layers were then allowed to cool to <70 °C before being returned to the analysis system for further STM characterization. Quantitative surface morphological analyses were performed by independently calculating the autocorrelation and height-height correlation functions for multiple STM micrographs for each surface, using the GWYDDION software package. This provided values for the average mound radius r_c and the rms surface roughness σ, which is also referred to as the surface width. The latter values are in good agreement with the values determined using the Omicron SCALA® software. The uncertainty in the parameters r_c and σ are estimated by independently analyzing a set consisting of a minimum of six micrographs obtained from different regions of the same sample surface. For example, the value for σ for an as-grown surface with t=60 nm is 1.2 ± 0.2, where 0.2 represents the standard deviation in σ from *different areas* of the same sample. This variation in surface morphology at different places of the same sample is comparable to the variation between different samples: For the same experimental conditions as above, the average σ-value from five independently grown layers is 1.29 ± 0.14, where 0.14 is the standard deviation associated with the analysis from *different samples*. Therefore, throughout this study we assume that the variation in morphology on a single surface represents the "true" morphological variability, i.e., experimental uncertainty.

III. RESULTS

All Cu layers are complete single crystals, with a cube-on-cube epitaxial relationship with the substrate, $(001)_{\mathrm{Cu}}\|(001)_{\mathrm{MgO}}$ and $[001]_{\mathrm{Cu}}\|[001]_{\mathrm{MgO}}$, as determined by x-ray diffraction and cross-sectional SEM analyses. This is consistent with our previous study on the epitaxial growth of Cu/MgO(001).[10,19] The following results focus on comparing the surface morphology of as-grown (T_s=100 °C) and annealed (T_a=200 and 300 °C) Cu layers with thicknesses t=24, 60, and 120 nm. For consistency purposes, the presented micrographs, as well as the quantitative surface morphological analyses, are from the same representative sample set. That is, the data for a given thickness from the as-grown and annealed surfaces are from the *identical* sample, obtained in a single multistep experiment. Annealing at higher temperatures T_a=400–700 °C leads to partial oxidation at the Cu–MgO interface and thermodynamically driven Cu islanding to minimize the layer-substrate interface area. These high-T_a results are not presented here, as they involve substrate effects that are beyond the scope of this paper, which focuses on the morphological evolution of pure Cu surfaces.

Figure 1(a) is a typical *in situ* scanning tunneling micrograph from a $500\times 500\ \mathrm{nm}^2$ surface area of an as-deposited 120-nm-thick Cu(001) layer. The surface exhibits elliptically shaped mounds with an average width w of 80 ± 10 nm and a peak-to-valley height h of 3.7 ± 0.3 nm, corresponding to a σ value of 1.3 ± 0.1 nm. Some mounds are elongated along the [110] or $[\bar{1}10]$ directions. This is attributed to mound coalescence, which occurs preferentially along ⟨110⟩ directions. Similar mound elongation along perpendicular ⟨110⟩ directions has been previously reported for the epitaxial growth of cubic materials on MgO(001) including Cu,[2,10] TiN,[26] and CrN,[27–29] and has been attributed to an anisotropic surface diffusion and/or an anisotropy in the step edge energies and two-dimensional adatom adsorption on islands.

Figure 1(b) is a $500\times 500\ \mathrm{nm}^2$ micrograph from the same 120-nm-thick Cu layer, which has been successively annealed at 200 and 300 °C for 30 min each. The mounds have a measured average width of 78 ± 6 nm, which is, within experimental uncertainty, equal to w of the as-grown layer. The annealed mounds exhibit a considerably larger shape anisotropy compared to the as-deposited structures. They also have a 1.3-times smaller height h=2.8 ± 0.4 nm, corresponding to σ=1.0 ± 0.1 nm. The average mound

Author complimentary copy. Redistribution subject to AIP license or copyright, see http://jap.aip.org/jap/copyright.jsp

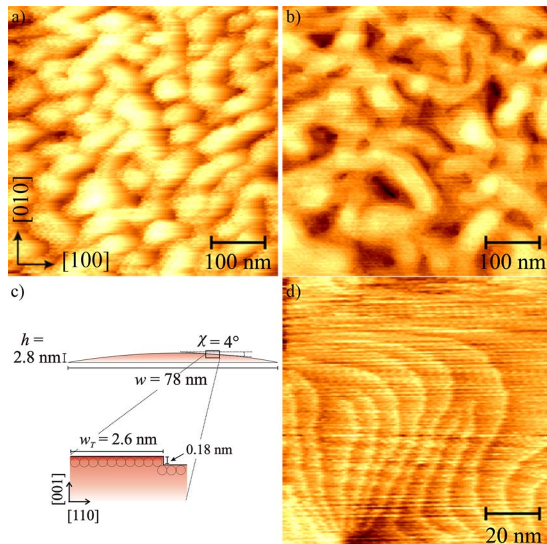

FIG. 1. (Color online) *In situ* scanning tunneling micrographs from a 120-nm-thick Cu(001)/MgO(001) layer: (a) as deposited and (b) after subsequent anneals at 200 and 300 °C for 30 min each. (c) Schematic illustrating the mound dimensions and terrace structure corresponding to the surface in (b). (d) Higher magnification micrograph from the same surface as in (b).

structure of the annealed surface is schematically illustrated in Fig. 1(c). The average slope angle $\chi=4°$ is determined from the peak-to-valley height and the mound radius $r_c=w/2$, using $\chi=\tan^{-1}(h/r_c)$.[10] This value is slightly smaller than the corresponding $\chi=5°$ for the as-grown surface, indicating that annealing reduces the slope of surface mounds. We also determine the average terrace width w_T using χ and the step height $h_{001}=a/2=0.18$ nm along the vertical $\langle 001\rangle$ direction, where $a=0.3615$ nm is the Cu lattice constant.[13,15] w_T increases from 1.7 to 2.6 nm, corresponding to an average terrace width of 7 and 10 atoms for the as-grown and annealed surfaces, respectively. The latter values assume a horizontal $\langle 110\rangle$ close-packed direction with an interatomic spacing of $a/\sqrt{2}=0.25$ nm.

The atomically smooth terraces can be directly observed in higher magnification images of particularly smooth surface areas, such as the one shown in Fig. 1(d). This is a 100×100 nm^2 micrograph from this same layer after successive anneals at 200 and 300 °C. The bright lines correspond to steps that are, based on line-scan analyses, single-atom high. That is, the areas between the lines are atomically smooth surfaces, which are, on average, 6 ± 2 nm wide in this micrograph. This value is larger than the large-area average value $w_T=2.6$ nm obtained from the slope-angle calculation. This difference is simply due to the choice of the micrograph shown in Fig. 1(d), which is from a particularly smooth area so that the atomic-height steps are easily observable. Atomic-height steps cannot be resolved in steeper portions of the surface, as near the top of the micrograph in Fig. 1(d).

Figure 2 shows STM micrographs from an as-deposited and annealed Cu(001) layer that is five times thinner than that shown in Fig. 1. The as-deposited surface shown in Fig. 2(a) exhibits approximately circular mounds, which are 60 ± 20 nm wide, 3.6 ± 0.4 nm high, and have an average slope of $\chi=7°$. Comparing these values to those from Fig. 1(a) indicates that increasing layer thickness leads to an increase in w, while h remains approximately constant. This is primarily attributed to coalescence during growth, which causes mounds to broaden and acquire anisotropic shapes, without significantly affecting their height.

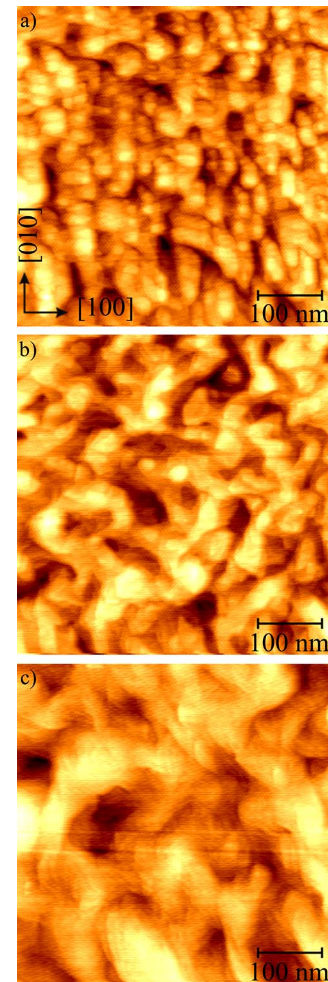

FIG. 2. (Color online) *In situ* scanning tunneling micrographs from 500×500 nm^2 areas of a 24-nm-thick Cu(001) layer (a) as deposited, (b) after a 30 min anneal at 200 °C, and (c) after a subsequent 30 min anneal at 300 °C.

Figure 2(b) is a micrograph from the same 24-nm-thick layer after a 30 min vacuum anneal at 200 °C. The surface morphology now consists of broader elliptical mounds, which have a tendency to elongate along perpendicular [110] and $[\bar{1}10]$ directions, comparable to those from the 120-nm-thick annealed layer. The mounds have an average width of 80 ± 20 nm and a peak-to-valley height of 3.0 ± 0.2 nm, which corresponds to a rms surface roughness of 1.08 ± 0.06 nm. The mound slope is reduced to $\chi=4°$, corresponding to an average terrace length of 2.6 nm. Figure 2(c) shows the surface morphology after a subsequent anneal at 300 °C for 30 min. The mounds have further broadened to reach an average width of 140 ± 40 nm. In addition, the mound height has continued to decrease, with $h=2.1\pm 0.2$ nm and $\sigma=0.74\pm 0.08$ nm. The overall effect of the annealing is an increase in width and a decrease in height, which results in a reduction of χ from 7° to 2° and an increase in w_T from 1.6 to 6.3 nm.

Author complimentary copy. Redistribution subject to AIP license or copyright, see http://jap.aip.org/jap/copyright.jsp

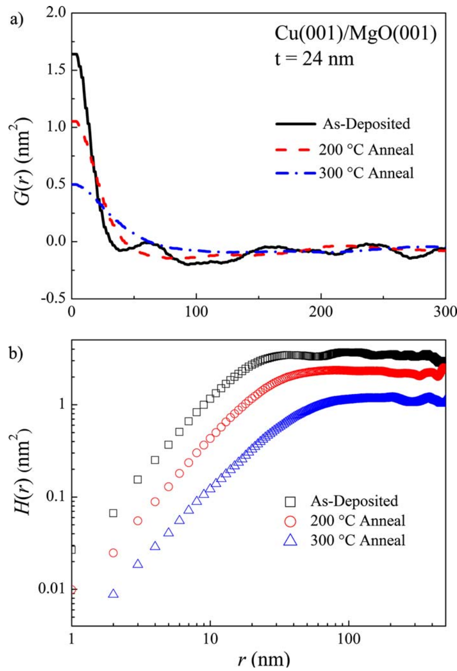

FIG. 3. (Color online) (a) Autocorrelation function $G(r)$ and (b) height-height correlation function $H(r)$ from the as-deposited and annealed surfaces of a 24-nm-thick Cu(001) layer.

The surface morphology is quantitatively analyzed using the autocorrelation function $G(r)$ and the height-height correlation function $H(r)$. For statistical purposes, $G(r)$ and $H(r)$ are calculated for a minimum of six independently acquired micrographs from randomly chosen surface areas for each temperature and layer thickness. $G(r)$ is defined as

$$G(r) = \langle [h(r_1)h(r_2)] \rangle, \tag{1}$$

where $r=r_1-r_2$ is the distance between positions r_1 and r_2, and $h(r_1)$ and $h(r_2)$ are the heights at r_1 and r_2, respectively.[3,12,30] Exemplary $G(r)$ curves are plotted in Fig. 3(a) for a 24-nm-thick as-deposited and annealed layer. The curves show a finite value at $r=0$, which corresponds to the mean square roughness. That is, the surface width σ, or rms surface roughness, is directly obtained from the relation $\sigma = \sqrt{G(0)}$.[12] As r increases, the heights at r_1 and r_2 become less correlated, so that $G(r)$ decreases and ultimately approaches zero for $r \to \infty$, as observed in Fig. 3(a). The position where $G(r)$ intercepts the x-axis corresponds to the mound radius r_c. The mound width is, in turn, directly obtained from r_c using $w=2r_c$. When comparing the three $G(r)$ plots in Fig. 3(a), it is evident that annealing causes $G(0)$ to decrease and the x-axis intercept to increase. That is, annealing reduces σ and increases r_c, yielding considerably flatter surface mounds as described above for Fig. 2 and quantitatively discussed below using Fig. 4.

Figure 3(b) is a log-log plot of the height-height correlation function $H(r)$ for the same surfaces used for Fig. 3(a). $H(r)$ provides insight into the scaling characteristics of a rough surface and is given by

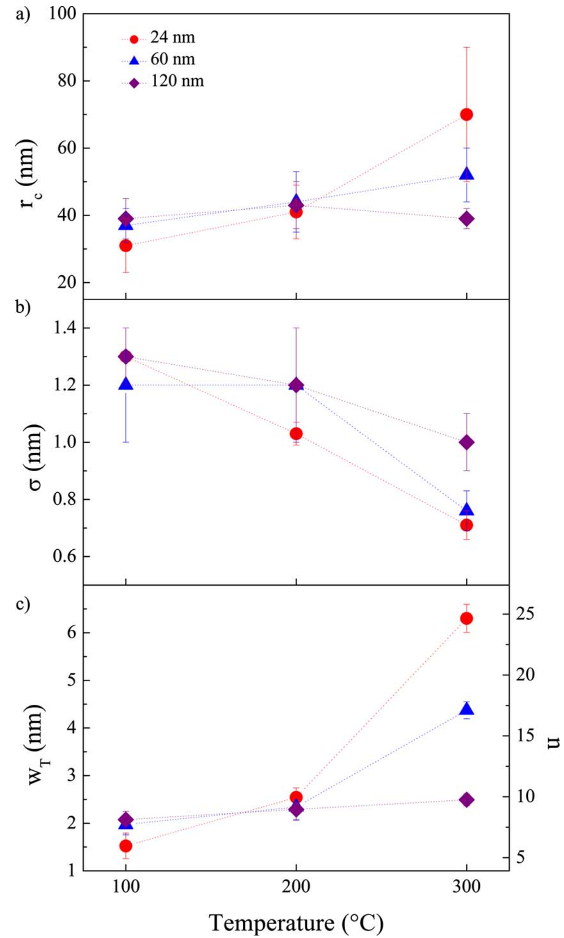

FIG. 4. (Color online) (a) Mound radius r_c, (b) interface width σ, and (c) average terrace width w_T as a function of temperature for Cu(001) layers with thicknesses t=24, 60, and 120 nm. Here, 100 °C refers to growth temperature and 200 and 300 °C refer to annealing temperatures. The right y-axis in (c) indicates the terrace width in number of atoms n.

$$H(r) = \langle [h(r) - h(0)]^2 \rangle = 2\sigma^2 f\left(\frac{r}{\xi}\right), \tag{2}$$

where ξ is the lateral correlation length, which defines the scale over which h is correlated. The scaling function $f(r/\xi)$ follows a power law $f=(r/\xi)^{2\alpha}$ for small r ($\ll \xi$) and is equal to unity for large r ($\gg \xi$),[31,32] that is, $H(r \to \infty) = 2\sigma^2$.[33] Values for ξ, σ, and the scaling exponent α are determined from a fit through the experimental $H(r)$ data for each layer thickness and annealing condition. All layers exhibit α-values between 0.79 and 0.84, with an average of 0.82 ± 0.03, which does not change with annealing. These values are within the range $0 \leq \alpha < 1$, which is characteristic of a self-affine fractal surface morphology where the scaling is anisotropic between the vertical and lateral directions.[34] $H(r)$ reaches a first maximum at $r=r_c$. The values for r_c and σ obtained from $H(r)$ are in good agreement with those obtained using $G(r)$ and are presented in Fig. 4.

Figure 4(a) is a plot of the mound radius as a function of temperature T for three Cu(001) layers with thicknesses t =24, 60, and 120 nm. Here, T=100 °C refers to the as-deposited layers and T=200 and 300 °C refer to the layers annealed at 200 and 300 °C, respectively. The error bars represent the standard deviation of r_c values determined from

Author complimentary copy. Redistribution subject to AIP license or copyright, see http://jap.aip.org/jap/copyright.jsp

a set of at least six independent STM images. For all layers, r_c is smallest for the as-deposited surface and increases with annealing. This effect is most pronounced for $t=24$ nm, where r_c increases by more than a factor of 2 from 31 ± 8 to 70 ± 20 nm for $T=100$ and 300 °C, respectively. This is consistent with the qualitative discussion above, describing the strong surface morphological difference between the surfaces shown in Figs. 2(a) and 2(c). Annealing becomes less effective as the layer thickness is increased to $t=60$ nm, and r_c becomes nearly independent of annealing for $t=120$ nm. For the case of the as-deposited surfaces, r_c increases with t, which is attributed to mound coalescence, as discussed above. However, this trend is reversed for annealed surfaces ($T_a=300$ °C) since the effect due to annealing decreases with t. Consequently, the largest r_c value is observed for the thinnest layer annealed at the highest temperature.

Figure 4(b) is a plot of the average rms surface roughness σ versus temperature for $t=24$, 60, and 120 nm. σ values of the as-deposited surfaces are nearly independent of thickness and decrease with annealing for all layers. This effect is most dramatic for $t=24$ nm, where σ decreases from 1.3 ± 0.1 to 0.74 ± 0.08 nm for $T=100$ and 300 °C, respectively, corresponding to a reduction in the roughness, and therefore also the mound height, by a factor of 1.8. Annealing of the thicker layers results in decreases in σ by factors of 1.5 and 1.4 for $t=60$ and 120 nm, respectively.

The plot in Fig. 4(c) shows the average terrace width w_T, as determined from r_c and σ values plotted in Figs. 4(a) and 4(b), respectively. The y-axis on the right in Fig. 4(c) indicates the corresponding number of atoms n along a close-packed ⟨110⟩ direction, as also illustrated in Fig. 1(c). For the as-deposited surfaces, w_T increases with t, from 1.5 nm for $t=24$ nm to 2.1 nm for $t=120$ nm, corresponding to terraces that consist of an average of $n=6-8$ atoms per step. Annealing yields an increase in w_T for all layers. As expected from the results above, this effect is strongest for $t=24$ nm for which w_T increases by a factor of 4 from 1.5 to 6.3 nm, corresponding to $n=6$ and 25 atoms for $T=100$ and 300 °C, respectively. In contrast, the terrace width increases by only 20%, from 8 to 10 atoms, after annealing of the 120-nm-thick layer.

IV. DISCUSSION

The summary plots in Fig. 4 show the effect of annealing on the surface morphology of epitaxial Cu(001) layers. The overall observed trend is a smoothening of the surfaces due to both an increase in the average mound width and a decrease in the mound height, as quantified by r_c and σ, respectively. This smoothening is attributed to a thermodynamically driven mass transport, through surface diffusion, which reduces the overall surface area and the density of surface steps that are expected to be energetically less favored in comparison to a smooth (001) surface. In addition, the plots indicate that the mass transport during annealing is strongly affected by the layer thickness. In particular, the thinnest layer, which initially has the highest average surface slope and step density, smoothens faster than the thickest layer with the flattest initial surface. This can be attributed to the higher step density, which represents a higher driving force for surface mass transport for the thinnest layer. Based on this argument, the surface morphologies and, in particular, the average terrace width for different layer thicknesses should converge during annealing. However, in direct contradiction to this argument, Fig. 4(c) shows that annealing at 300 °C causes the surface with the shortest initial terrace width to exhibit the largest final terrace width. This suggests that the surface morphological evolution during annealing follows different pathways for the thin versus thick layers. Some insight regarding the differences are provided by the STM micrographs: The small circular mounds in Fig. 2(a) of the 24-nm-thick layer develop during annealing into fewer wider mounds shown in Figs. 2(b) and 2(c) by a competitive coalescence process where some mounds grow at the expense of their smaller neighbors, which provide atoms and are ultimately consumed. In contrast, annealing of the already broader mounds from the 120-nm-thick layer in Fig. 1(a) results in neighbors joining and developing into elliptical mounds that elongate along orthogonal ⟨110⟩ directions. In this case, the larger initial mound width results in a higher "mound stability" during annealing, so that only a few mounds disappear, which, in turn, limits the available mass for lateral mound growth and surface smoothening. That is, the initially wider mound width for the thickest layer leads to a quasistable surface morphology that exhibits anisotropic surface mounds but limits further smoothening and stabilizes the surface step density. It would be interesting to quantify the stability of this surface morphology using considerably longer (one to two orders of magnitude) annealing times. However, oxygen background impurity considerations would make the results of such experiments less reliable than experiments with variable T_a, as done in the present study.

V. CONCLUSIONS

Single crystal Cu(001) layers grown on MgO(001) by magnetron sputter deposition at $T_s=100$ °C exhibit self-affine surface mounds, which increase in width as a function of layer thickness from 60 ± 20 to 80 ± 10 nm for $t=24$ and 120 nm, respectively, while the mound height remains nearly constant. *In situ* vacuum annealing at 200 and 300 °C results in mound broadening, which is most pronounced for the thinnest $t=24$ nm layer, resulting in a decrease in the average surface slope χ from 7° to 2° and an increase in the average terrace width w_T by more than a factor of 4. This is attributed to competitive mound coalescence during annealing, which causes some mounds to grow at the expense of their smaller neighbors that are consumed. In contrast, χ remains nearly constant during annealing of the 120-nm-thick layer and w_T increases by only 20%. This limited effect for the thicker layer is the result of the smooth initial surface that causes mounds to join along perpendicular ⟨110⟩ directions to form a quasistable anisotropic morphology that exhibits only limited mass transport at 300 °C. The somewhat surprising conclusion is that annealing causes the initially roughest surface to become the smoothest. That is, to achieve the lowest Cu(001) surface roughness within the experimen-

Author complimentary copy. Redistribution subject to AIP license or copyright, see http://jap.aip.org/jap/copyright.jsp

tal constraints of this study, a high roughness of the as-deposited surface is desirable.

ACKNOWLEDGMENTS

This research was funded by the Semiconductor Research Corporation and New York State through the Center for Advanced Interconnect Systems Technologies under Contract Nos. 1292.004 and 1292.036.

[1]T. Mewes, M. Rickart, A. Mougin, S. O. Demokritov, J. Fassbender, B. Hillebrands, and M. Scheib, Surf. Sci. **481**, 87 (2001).
[2]G. Eilers and K. Mukasa, Jpn. J. Appl. Phys., Part 1 **39**, 3780 (2000).
[3]B. W. Karr, Y. W. Kim, I. Petrov, D. B. Bergstrom, D. G. Cahill, and J. E. Greene, J. Appl. Phys. **80**, 6699 (1996).
[4]V. Musolino, A. Dal Corso, and A. Selloni, Phys. Rev. Lett. **83**, 2761 (1999).
[5]X. Yang and S. S. Perry, Surf. Sci. **506**, L261 (2002).
[6]F. Reniers, M. P. Delplancke, A. Asskali, V. Rooryck, and O. Van Sinay, Appl. Surf. Sci. **92**, 35 (1996).
[7]H. S. Goindi, C. S. Shin, M. Frederick, Y. Shusterman, H. Kim, I. Petrov, and G. Ramanath, in *Growth, Evolution and Properties of Surfaces, Thin Films and Self-Organized Structures*, MRS Symposia Proceedings No. 648, edited by S. C. Moss (Materials Research Society, Pittsburgh, PA, 2001), p. 11.37.
[8]H. Bialas and K. Heneka, Vacuum **45**, 79 (1994).
[9]E. T. Krastev, L. D. Voice, and R. G. Tobin, J. Appl. Phys. **79**, 6865 (1996).
[10]J. M. Purswani and D. Gall, Thin Solid Films **516**, 465 (2007).
[11]R. A. Lukaszew and R. Clarke, Appl. Surf. Sci. **191**, 118 (2002).
[12]A. Meunier, B. Gilles, and M. Verdier, J. Cryst. Growth **275**, 1059(E) (2005).
[13]H. Jiang, T. J. Klemmer, J. A. Barnard, and E. A. Payzant, J. Vac. Sci. Technol. A **16**, 3376 (1998).
[14]I. Hashim, B. Park, and H. A. Atwater, in *Evolution of Surface and Thin-Film Microstructure*, MRS Symposia Proceedings No. 280, edited by H. A. Atwater, E. H. Chason, M. L. Grabow, and M. G. Lagally (Materials Research Society, Pittsburgh, PA, 1993), p. 327.
[15]I. Hashim, B. Park, and H. A. Atwater, Appl. Phys. Lett. **63**, 2833 (1993).
[16]B. G. Demczyk, R. Naik, G. Auner, C. Kota, and U. Rao, J. Appl. Phys. **75**, 1956 (1994).
[17]T. I. M. Bootsma and T. Hibma, Surf. Sci. **331–333**, 636 (1995).
[18]J. B. Zhou and T. Gustafsson, Surf. Sci. **375**, 221 (1997).
[19]J. M. Purswani, T. Spila, and D. Gall, Thin Solid Films **515**, 1166 (2006).
[20]J.-W. He and P. J. Møller, Surf. Sci. **178**, 934 (1986).
[21]M. P. Delplancke, P. Delcambe, L. Binst, M. Jardinier-Offergeld, and F. Bouillon, Thin Solid Films **143**, 43 (1986).
[22]E. F. McCullen, C.-L. Hsu, and R. G. Tobin, Surf. Sci. **481**, 198 (2001).
[23]E. B. Svedberg, P. Sandström, J.-E. Sundgren, J. E. Greene, and L. D. Madsen, Surf. Sci. **429**, 206 (1999).
[24]R. C. Powell, N.-E. Lee, Y.-W. Kim, and J. E. Greene, J. Appl. Phys. **73**, 189 (1993).
[25]J. R. Frederick, J. D'Arcy-Gall, and D. Gall, Thin Solid Films **494**, 330 (2006).
[26]C.-S. Shin, S. Rudenja, D. Gall, N. Hellgren, T.-Y. Lee, I. Petrov, and J. E. Greene, J. Appl. Phys. **95**, 356 (2004).
[27]D. Gall, C.-S. Shin, T. Spila, M. Odén, M. J. H. Senna, J. E. Greene, and I. Petrov, J. Appl. Phys. **91**, 3589 (2002).
[28]J. R. Frederick and D. Gall, Appl. Phys. Lett. **87**, 053107 (2005).
[29]J. R. Frederick and D. Gall, J. Appl. Phys. **98**, 054906 (2005).
[30]G. Rasigni, F. Varnier, M. Rasigni, J. P. Palmari, and A. Llebaria, Phys. Rev. B **25**, 2315 (1982).
[31]H.-N. Yang and T.-M. Lu, Phys. Rev. B **51**, 2479 (1995).
[32]H.-N. Yang, A. Chan, and G.-C. Wang, J. Appl. Phys. **74**, 101 (1993).
[33]K. Vanormelingen, B. Degroote, and A. Vantomme, J. Vac. Sci. Technol. B **24**, 725 (2006).
[34]B. B. Mandelbrot, *The Fractal Geometry of Nature* (Freeman, New York, 1982).

Author complimentary copy. Redistribution subject to AIP license or copyright, see http://jap.aip.org/jap/copyright.jsp